Enhancing the dark side: Asymmetric gain of cone photoreceptors underpins discrimination of visual scenes based on their skewness.

Matthew Yedutenko[1], Marcus H.C. Howlett[1], and Maarten Kamermans[1, 2]

[1]Retinal Signal Processing Lab, Netherlands Institute for Neuroscience, Amsterdam, Netherlands
[2]Department of Biomedical Physics and Biomedical Optics, Amsterdam University Medical Center, University of Amsterdam, Amsterdam, Netherlands

Abbreviated Tittle: Cone responses to skewness

Corresponding Author: Maarten Kamermans, m.kamermans@nin.knaw.nl

10 Figures

1 Table

Funding

This work was supported by a ZonMW grant 91215062 (M.K.), a grant from Horizon 2020: "Switchboard" (M.K.), a grant of ODAS (M.K.) and a grant of the Foundation of Friends of the NIN (M.K.).

Abstract

Psychophysical data indicates humans can discriminate visual scenes based on their skewness – the ratio of dark and bright patches within a visual scene. It was also shown that on a phenomenological level this skew discrimination is described by the so-called Blackshot mechanism, which accentuates strong negative contrasts within a scene. Here we demonstrate that the Blackshot mechanism is implemented by the asymmetric gain of the cone phototransduction cascade, which is higher for strong negative contrasts than for strong positive contrasts. We recorded from goldfish cone photoreceptors and found that the asymmetry in the phototransduction gain leads to higher amplitude of the responses to negatively than to positively skewed light stimuli. This asymmetry in the amplitude was present in the photocurrent, voltage response and cone synaptic output. These results highlights the importance of the early photoreceptor non-linearity for the perception.

Additionally, we found that stimulus skewness leads to a subtle change in photoreceptor kinetics. For negatively skewed stimuli, the cone's impulse response functions peak later than for positively skewed stimulus. However, stimulus skewness does not affect the cone's overall integration time.

Introduction

Psychophysical studies show that humans are sensitive to the ratio of negative (intensity lower than the mean) and positive (intensity higher than the mean) patches of contrast in visual scenes (Chubb *et al.*, 1994, 2004; Graham *et al.*, 2016). This ratio is described by the parameter known as skewness. Visual stimuli are called positively skewed if there is a predominance of negative contrasts with some infrequent patches of high positive contrast and are called negatively skewed when the situation is reversed. Figure 1 illustrates one's ability to discriminate visual scenes based on skewness by mimicking an experiment performed by Chubb et al. (1994,

2004). The textures were randomly drawn from two distributions equal in every aspect but skewness (Bonin *et al.*, 2006). Yet, one can appreciate the clear difference between negatively skewed images (right upper) and positively skewed images (remaining panels). Chubb et al. (1994, 2004) showed that on a phenomenological level the sensitivity to skewness can be described by the so-called Blackshot mechanism. This Blackshot mechanism does not react to skewness per se, rather its sensitivity to strong negative contrasts is simply much higher than to strong positive contrasts and so it effectively reports the fraction of strong negative contrasts within the scene.

What are the neuronal correlates of the Blackshot mechanism? Studies using salamander retinal ganglion cells (RGC) (Tkačik *et al.*, 2014) and cat lateral geniculate nucleus neurons (LGN) (Bonin *et al.*, 2006) did not report any response differences associated with changes in stimulus skewness. Therefore, both studies concluded that the discrimination between skewed stimuli occurs in the visual cortex. On the other hand, it is well-established that the retinal photoreceptor's gain is asymmetric: given an equal input magnitude, the response amplitude to a strong (>0.4 Weber unit) negative contrast step is greater than it is to a strong positive contrast step (Laughlin, 1981; van Hateren, 2005; Endeman & Kamermans, 2010; Baden *et al.*, 2013; Angueyra *et al.*, 2021*a*). Furthermore, this responses asymmetry is observed throughout the

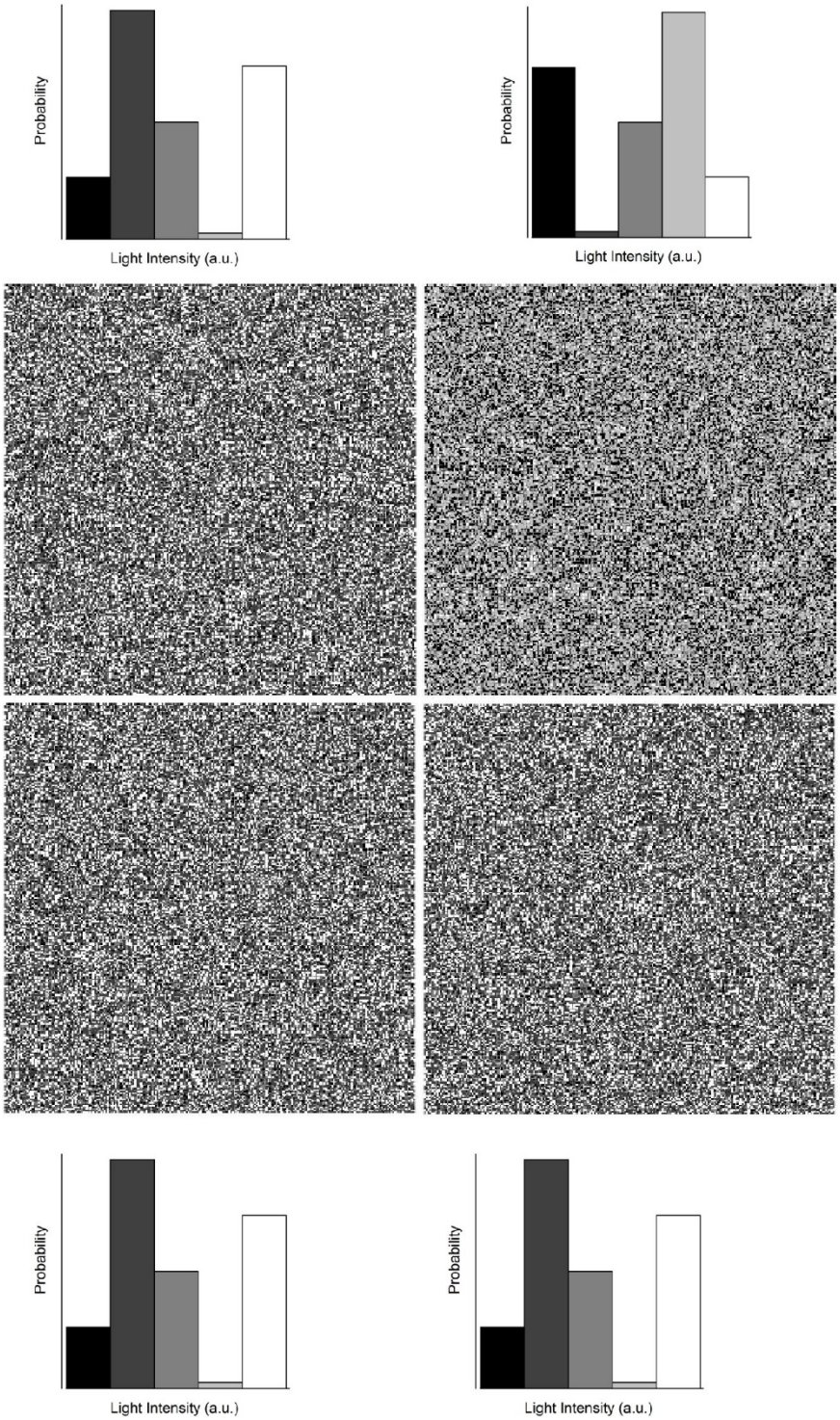

Figure 1

The discrimination of skewed stimuli. An example of textures used by Chubb et al.(1994, 2004) to psychophysically probe the ability of humans to discriminate visual scenes based on their skewness. The textures were randomly drawn from the probability distributions adjacent to each panel following the approach described by Bonin et al. (2006) and differed only in terms of skewness. The upper right texture is negatively skewed (-0.4), the remainder are positively skewed (+0.4).

post-receptor retinal stages (Lee *et al.*, 2003; Zaghloul *et al.*, 2003), the LGN (Kremkow *et al.*, 2014), and the primary visual cortex (Zemon *et al.*, 1988; Jin *et al.*, 2008; Yeh *et al.*, 2009; Kremkow *et al.*, 2014). The asymmetrical processing of positive and negative contrasts should lead to different response amplitudes to negatively and positively skewed stimuli and thus might underpin the discrimination of skewed stimuli.

A possible reason why the differences in responses to skewed stimuli were not found in RGC (Tkačik *et al.*, 2014) and LGN (Bonin *et al.*, 2006) studies was the power spectra of the stimuli used. In both cases, the researchers employed band-limited white noise, where large proportions of the signal power are outside the photoreceptor frequency bandwidth. Thus, in both studies temporal filtering discarded a significant portion of the signal, reducing the skewness and amplitude of the "effective" light stimuli actually available to photoreceptors. Consequently, Bonin et al. (2006) and Tkacik et al. (2014) may not have found significant differences in the processing of skewed stimuli because a) their stimuli hardly differed in terms of "effective" skewness and b) the "effective" amplitudes of the employed stimuli were too low to drive cone photoreceptors outside their linear response range.

Here we address whether photoreceptors process positive and negative skewed stimuli differently. To account for the kinetics of cone photoreceptors, we stimulated goldfish cones with sets of skewed stimuli with bandwidth similar to those of the goldfish cones. We found the asymmetry in goldfish photoreceptor gain does indeed entail skew-dependent changes in the cone response, leading to greater response amplitudes to negatively than to positively skewed stimuli. This asymmetry originates in the cone phototransduction cascade and implements the Blackshot mechanism. Additionally, we found that the cone's impulse response function peaks ≈ 3.6 ms later for negatively skewed stimuli whereas the cone's integration time is unaffected by stimulus skewness.

Thus, we show that in contrast to what is often implied in the models of the various retinal, thalamic and cortical neurons (Carandini *et al.*, 2005; Schreyer & Gollisch, 2021), cone photoreceptors do not simply linearly relay visual stimuli to the downstream circuitry, but also emphasize specific features of those stimuli. These results highlight the necessity of the account for a full non-linear character of the photoreceptor signal processing in studies of the visual system.

Materials and Methods

Recording procedures

All animal experiments were conducted under the responsibility of the ethical committee of the Royal Netherlands Academy of Arts and Sciences (KNAW), acting in accordance with the European Communities Council Directive of 22 July 2003 (2003/65/CE) under license number AVD-801002016517, issued by the Central Comity Animal Experiments of the Netherlands. In all experiments retinas of adult goldfish (*Carassius auratus*) were used.

Goldfish were first dark-adapted for 5-10 minutes, sacrificed and the eyes enucleated. Retinas were isolated under dim red illumination then placed photoreceptor side up in a recording chamber (300 µl, model RC-26G, Warner Instruments) mounted on a Nikon Eclipse 600FN microscope. The preparation was viewed on an LCD monitor by means of a 60× water-immersion objective (N.A. 1.0, Nikon), a CCD camera, and infrared ($\lambda > 800$ nm; Kodak wratten filter 87c, United States) differential interference contrast optics. Tissue was continuously superfused with oxygenated Ringer's solution at room temperature (20˚C). The composition of Ringer's solution was (in mM): 102.0 NaCl, 2.6 KCl, 1.0 $MgCl_2$, 1.0 $CaCl_2$, 28.0 $NaHCO_3$, 5.0 glucose continuously gassed with 2.5% CO_2 and 97.5% O_2 to yield a pH of 7.8 (osmolarity 245–255 mOsm). For calcium current (I_{Ca}) measurements, 5 mM of NaCl was substituted with 5mM of CsCl and 100 µM of niflumic acid added.

Measurements from goldfish cones were performed in current- (voltage response), and voltage- (photocurrent), clamp configurations. Patch pipettes (resistance 7-8 MOhm, PG-150T-10; Harvard Apparatus, Holliston, Massachusetts) were pulled with a Brown Flaming Puller

122 (Model P-87; Sutter Instruments Company). Patch pipette solution contained (in mM): 96 K-
123 gluconate, 10 KCl, 1 MgCl2, 0.1 CaCl2, 5 EGTA, 5 HEPES, 5 ATP-K2, 1 GTP-Na3, 0.1
124 cGMP-Na, 20 phosphocreatine-Na2, and 50 units ml^{-1} creatine phosphokinase, adjusted with
125 KOH to pH 7.27–7.3 (osmolarity 265–275 mOsm). The chloride equilibrium potential (E_{Cl})
126 was -55mV except when the calcium current (I_{Ca}) was studied. Here E_{Cl} was set at -41 mV by
127 changing the concentrations of K-gluconate and KCl to 87 and 19 mM, respectively. All
128 chemicals were supplied by Sigma-Aldrich (Zwijndrecht, the Netherlands), except for NaCl
129 (Merck Millipore, Amsterdam, the Netherlands).

130 Filled patch pipettes were mounted on a MP-85 Huxley/Wall-type manual micromanipulator
131 (Sutter Instrument Company) and connected to a HEKA EPC-10 Dual Patch Clamp amplifier
132 (HEKA Elektronik GmbH, Lambrecht, Germany). After obtaining a whole cell configuration,
133 cones were first spectrally classified then stimulated with a set of skewed stimuli of
134 corresponding chromaticity. Data were recorded at a sample rate of 1 kHz using Patchmaster
135 software package (HEKA Elektronik GmbH). In total, we recorded 14 cones in voltage-clamp
136 mode (8 light responses, 6 measurements of I_{Ca}) and 16 cones in current-clamp mode (all light
137 responses). The liquid junction potential (approximately -15 to -16 mV) was not compensated.

138 Light stimuli

139 The light stimulator was a custom-built LED stimulator with a three-wavelength high-intensity
140 LED (Atlas, Lamina Ceramics, Westhampton, New Jersey, US). The peak wavelengths were
141 465, 525 and 624 nm. Bandwidth was smaller than 25 nm. Linearity was ensured by an optical
142 feedback loop. The output of the LED stimulator was coupled to the microscope via an optic
143 fiber and focused on cone outer segments though a 60× water-immersion objective. The mean
144 light intensity of all stimuli was $1.2*10^4$ photons/μm^2/s, which is in the photopic level for
145 goldfish (Malchow & Yazulla, 1986). Stimuli were presented at 1 kHz.

Skew Stimulus Set#1. Skewed stimuli were based on the natural time series of chromatic intensities (NTSCI) from the Van Hateren library (Van Hateren *et al.*, 2002). Given that psychophysical studies indicated discrimination of the visual scenes based on the skewness in spatial domain (Figure 1), one might wonder whether it is appropriate to study phenomena which is spatial in nature with time series of intensities. However, such an approach is correct for the following two reasons. First of all, because of the saccades any spatial stimulus is converted into time series. So, photoreceptors did indeed perceived time series of intensities when in the psychophysical studies subjects were presented with the skewed textures. Secondly, the light response of the photoreceptor does not depend on the stimulus spatial structure, only on the light intensity within its outer segment. Hence, one can reproduce responses of the array of cones to a single presentation of texture by recording responses of the single cone to a time series of intensities.

The NTSCI power spectra is typical of that of 'natural stimuli' in that power declines as a function of frequency(Van Hateren, 1997; Van Hateren *et al.*, 2002; Frazor & Geisler, 2006). As a result of the predominance of lower frequencies, most of the light intensity changes throughout the NTSCI occur over timescales accessible to goldfish cones and previously the NTSCI has been used to unlock several non-linear performance features of cones (Endeman & Kamermans, 2010; Howlett *et al.*, 2017). To ensure that all aspects other than skewness remained equal, we first picked short stretches from the NTSCI that were positively skewed, then simply flipped these around the mean to generate negatively skewed stimuli.

To generate Stimulus set#1 we divided the NTSCI (Van Hateren *et al.*, 2002) into one-second long stretches. Then from each stretch we subtracted its minimum value, adjusted their mean light intensities to be equal and picked stretches with similar power spectra and root mean

square (r.m.s.), and median contrasts (between 0.23 and 0.25). The r.m.s. and median contrast for each stretch was calculated respectively as the ratio between the stretch's standard deviation and its mean, and the ratio between its deviation from the median, and its median. To ensure an absolute similarity between positively and negatively skewed stimuli, we selected only stretches where the maximum value was not larger than 2 times the mean. Next, we chose stretches with skewness's of 0.9, 1.6, 2.2. The skewness was calculated with the equation (1):

$$S = < \frac{(I - Imean)^3}{N\sigma^3} > \quad (\mathbf{1})$$

where N is the number of elements in the stretch, I corresponds to the light intensity of an element, I_{mean} and σ are mean and standard deviation within the stretch and brackets denotes averaging over the period.

We further narrowed our selection to three stretches all with similar power spectra (data not shown). Power spectra were calculated by Welch's averaged periodogram method (Welch, 1967). No window function was used, the length of the Fourier transform was same as the length of each corresponding data sequence. Total stimulus power was calculated as the integral under power spectra, the differences in the total stimulus power were no more than 10%. Finally, an additional pink noise stimulus with zero-skew and similar power spectra was added to the set. In total, Skew Stimulus set#1 consisted of seven 1-second stimuli.

Skew Stimulus set#2. This stimulus set consisted of three 4-second long stretches with a skewness of 2.2, 0, and -2.2. They were generated in the same way as the Skew Stimulus set#1, but with one additional condition: the degree of skewness delivered by the stimulus remained unchanged by the cone's temporal filtering. This was ensured by first convolving the NTSCI stretch with the mean photocurrent impulse response function (see below) obtained from responses to Skew Stimulus set #1. The skew of the convolution product, representing the "effective" stimulus, was then compared with the skew of the original stimulus (Figure 3). This

194 was further confirmed by determining the effective skewness after convolving the stimuli with
195 the impulse response function of each cone measured under Skew Stimulus set #2 conditions
196 (Figure 3B).

197 Calcium current isolation

198 To measure I_{Ca}, we used the mean voltage response (7 cells, 69 repeats in total) of cone
199 photoreceptors to Stimulus set #2 as the command voltages for the voltage clamp experiments.

200 To isolate I_{Ca} we followed the approach described by Fahrenhoft et al. (Fahrenfort *et al.*, 1999).
201 Briefly, to eliminate the calcium-dependent chloride current E_{Cl} was set at -41 mV and 100 µM
202 of niflumic acid added to the Ringer's solution; delayed rectifying, and hyperpolarization-
203 activated, potassium currents were blocked by substituting 5 mM of NaCl in Ringer's solution
204 with 5 mM of CsCl; light-activated conductances were saturated by a 20 µm spot of bright
205 white light focused on the cone outer segment; linear leak currents were removed by
206 subtraction. The leak current was estimated by clamping cones at -70mV, stepping to potentials
207 between -100 and 20 mV in 5 mV steps for 100 ms, calculating the mean current between 20
208 and 60 ms after the step onset, then determining the linear fit of the IV-relation between -100
209 and -60 mV (Vroman *et al.*, 2014; Kamar *et al.*, 2019).

210 Data analysis

211 For each cell, the skewness of its mean response to each stimulus was determined using
212 equation (1). In Figures 2, 3D and 8A, data was fitted using build-in Matlab least square
213 methods. All data analysis was performed in Matlab and Python.

214 Parallel cascade identification is the most rigorous method to describe the signal processing
215 properties of cone responses to naturalistic stimuli (Korenberg, 1991) . However, for practical
216 reasons our analysis only focuses on the estimation of the first parallel cascade, which is

effectively a linear filter followed by a static non-linearity. Apart from the computational and descriptive simplicity, this approach is also justifiable as it accurately describes cone responses, accounting for over 95% of the variance (Figure 8A).

The linear temporal filtering properties of a cone was described by its impulse response function. Impulse response functions were estimated as the inverse Fourier transform of the ratio between stimulus-response cross-power and stimulus power spectrum (Wiener, 1964; Kim & Rieke, 2001). The spectra were calculated using Welch averaged periodogram method (Welch, 1967). Stimuli and responses were detrended, divided into 500 ms long stretches, with 50% overlap, and windowed with a hamming function. The length of the Fourier transform was 1024 ms. Cone integration time was calculated as the integral of the impulse response function's initial polarization lobe (Daly & Normann, 1985).

To estimate the effective" stimuli perceived by each cone photoreceptors during each stimulus, we convolved the cone's impulse response function during that condition with the original light stimulus. Skews of these "effective" stimuli were calculated with equation (1). Discrepancies between the skewness of the "effective" stimuli and the skewness of the cone's responses, were considered a result of non-linear cone properties.

For "effective" Weber contrast steps (Figures 7&8A), light stimuli were first converted into Weber contrasts steps (Figure 7) with equation (2):

$$\mathrm{C} = \frac{(I - Imean)}{Imean} \quad (\mathbf{2})$$

These Weber contrast steps were then convolved with a mean impulse response function to obtain the "effective'' Weber contrast steps. The mean impulse response function used here was the averaged voltage-response derived impulse response function of all 16 cones measured in current clamp, which was subsequently scaled such that the integral under its curve yielded

one (Figure 7; Howlett et al., 2017). Even though a cone's impulse response function is affected by the skewness of the stimulus (Figure 8B&C), we used this mean impulse response function for the following reasons.

Firstly, observed changes to the impulse response function shape had little effect on the cone response dynamics. We convolved Skew Stimulus Set #2 with impulse response functions derived from responses to positive and negative stimulus of each of the cones (n=7) and found that the resulting convolution products were highly correlated ($r \approx 0.98 \pm 0.01$). Secondly, averaging across different stimulus skew conditions was crucial to account for biases in the estimate of the amplitude of the impulse response function arising from skewness of the light stimuli (Chichilnisky, 2001; Simoncelli *et al.*, 2004; Bonin *et al.*, 2006; Tkačik *et al.*, 2014). Finally, the goal of this analysis was to illustrate cone photoreceptor gain asymmetries rather than to provide a veridical description of the gain dependence on stimulus contrast.

To estimate the cone's non-linear gain function parameters we fitted the relationship between all the mean cone voltage responses and the "effective" Weber contrast steps (Figure 8A, 19000 data points) as the power function of input contrast (Van Hateren & Snippe, 2006) with equation 3:

$$\Delta V = a * (C + b)^d + e \quad (\mathbf{3})$$

Here ΔV denotes voltage response, C is the "effective" Weber contrast, a, b, d, and e are fit parameters. At the biophysical level b) corresponds to the baseline rate of phosphodiesterase activity (PDE), d) describes the inter-dependence between the PDE activity rate and the voltage response, e) is proportional to the baseline concentration of cyclic guanosine monophosphate and a) is a scaling factor (Van Hateren & Snippe, 2006). The quality of the fit was quantified with the adjusted coefficient of determination (R^2). The highest R^2 (0.95) was obtained using the following parameter values (value ± 95 % confidence interval): a=0.05138 ± 0.03506,

264 b=1.166 ± 0.072, d= -0.1251 ± 0.0959, e=-0.05046 ± 0.03552. Our estimation of the power
265 function (d) was close to that obtained by Van Hateren and Snippe (2006) in their theoretical
266 study.

267 Model

268 Photoreceptor responses were modelled in matlab using Van Hateren's model of vertebrate
269 photoreceptors (van Hateren & Snippe, 2007), which was shown to be remarkably precise in
270 capturing the processing steps involved in generating a cone's signal. Apart from the activation
271 of hyperpolarization-activated current (I_h; Howlett et al., 2017; Kamermans et al., 2017), the
272 model closely simulates all the cone's biophysical processing steps from the photon-initiated
273 activation of conopsins to the cGMP-regulated changes in the photocurrent, followed by the
274 generation of the voltage response. The model simulates cone photoreceptors as a cascade of
275 low-pass filters, a static (instantaneous and memoryless) non-linearity, and two divisive
276 feedback loops (van Hateren, 2005; van Hateren & Snippe, 2007). The low-pass filters
277 correspond to the kinetics of the different biophysical processing steps. The non-linearity
278 describes the inverse proportional dependence between light intensity and changes in the
279 cGMP concentration. The first feedback loop describes the regulation of the rate of cGMP
280 production by calcium influx through cGMP-gated channels. The second feedback loop
281 corresponds to the regulation of the membrane voltage by voltage-sensitive channels in the
282 cone inner segment. The cone's non-linear gain (Figure 8A) originates from the interplay
283 between the hydrolysis of the cGMP by PDE and calcium-regulated (feedback loop) production

of the cGMP by guanylyl cyclase (GC)

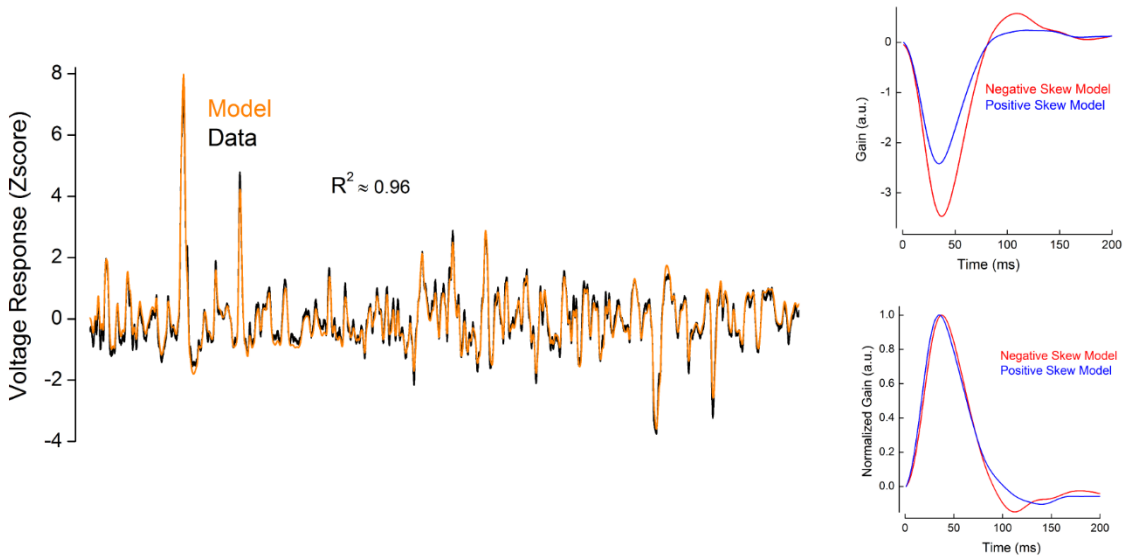

Figure 2

Example of the performance of the Van Hateren model for goldfish cones. Left. Voltage responses as Z-scores to Skew Stimulus set #2 for a representative recorded cone (black line) and for the simulated cone (orange line). The coefficient of determination (R^2) between these two traces was 0.98. Right. Impulse response functions obtained from the simulated responses to negatively (red) and positively (blue) skewed stimuli. Parameters for the simulation are listed in the Table 1.

We verified that the Van Hateren model could capture responses to skewed stimuli. For this we fitted the model to the voltage responses of 7 goldfish cones recorded under Skew Stimulus Set#2 conditions. The model parameters were modulated within the ranges determined by Endeman and Kamermans (2010) and are shown in the Table 1. For all 7 cells, the correlation coefficient between modelled and recorded voltage responses were no less than 0.97 (adjusted $R^2 \geq 0.94$ Figure 2). Moreover, the impulse response functions estimated from the simulated responses to positively and negatively skewed stimuli retained features of the impulse response functions derived from the recorded voltage responses. For example, for both recorded and simulated cone voltage responses, impulse response functions peaked 3 ms (8.5±1%, p=0.00013) later under the negatively skewed stimulus compared to the positively skewed

condition but showed no statistically significant difference in their full width at half maximum (FWHM), or in integration time (Figure 2). Thus, Van Hateren's model reproduces accurately cone responses to skewed stimuli.

Next, we used the Van Hateren model to estimate the "effective" stimuli perceived by salamander and cat cones in the studies by Tkacik et al. (2014) and Bonin et al. (2006), respectively. To model salamander cones we adjusted the parameters of Van Hateren's model such that the time course of the impulse response functions of simulated cones resembled those of salamander cones reported by Rieke (2001) and Baccus and Meister (2002). The exact simulation parameters are reported in the Table 1. Similarly, to model cat cones the Van Hateren model parameters were adjusted so that the impulse response function time course resembled the estimates made by Donner and Hemila (1996). For the cat, exact parameters of the simulation are reported in the Table 1.

"Light" stimuli mimicking those used by Bonin et al. and Tkacik et al. (2014) where respectively used to study the responses of the modelled cat (Figure 9) and salamander (Figure 10) cones to changes in skewness. The only difference was that for illustrative ease the positively and negatively skewed stimuli were mirror copies of each other. Cat stimuli had a r.m.s. contrast of 0.7, skews of ±0.4 and a flat power spectrum bandlimited to 124 Hz. Salamander stimuli had a r.m.s. contrast of 0.2, skews of ±2 and a flat power spectrum bandlimited to 30 Hz.

Statistics

All data are presented as mean ± SEM unless otherwise stated. Differences between groups were tested using two-tailed t-test (Student, 1908).

Results

Cone responses vary with skewness

Light responses of the photoreceptors are not affected by the stimulus spatial structure and depend only on the intensity of light which falls on the photoreceptor outer segment. Hence, one can reproduce responses of the array of cones to a single presentation of texture by recording responses of the single cone to a time series of intensities which compose those texture.

To assess the photoreceptor's contribution to skew discrimination, we exposed goldfish cones to a series of modified naturalistic time series of chromatic intensities (NTSCI) from the Van Hateren library (Van Hateren et al., 2002; Skew Stimulus set#1 in Material and Methods) and recorded their photocurrent and voltage responses (Figure 3A). Stimuli were equal in terms of mean intensity, root mean square contrast and median contrast, and had similar power spectra, while their skewness varied from -2.2 to +2.2. Positively and negatively skewed stimuli were mirror copies of each other, therefore any asymmetries between corresponding responses would reflect an asymmetry in the cone's processing.

To determine whether cones process negatively and positively skewed light stimuli differently, we plotted the skews of the photocurrent (Figure 3B) and voltage responses (Figure 3C) against the skews of the light stimuli. If there is no difference in processing, the skewness of the response will be equal to the light stimulus skewness and thus the data points will fall along a straight slope. However, if there is an asymmetry in the processing of positive and negative contrasts it would necessarily lead to the deviation of the data points from the grey line. Figures 3B&C shows that for positively skewed stimuli, the photocurrent and voltage responses are skewed to a lesser degree than are the light stimuli, whereas for the negatively skewed stimuli they are almost as equally skewed as the light stimuli. Note that the signal sign-inversion of

348 the voltage response also sign-inverts its skewness. Figures 3B&C indicate an asymmetry in
349 the processing of negatively and positively skewed stimuli by cone photoreceptors.

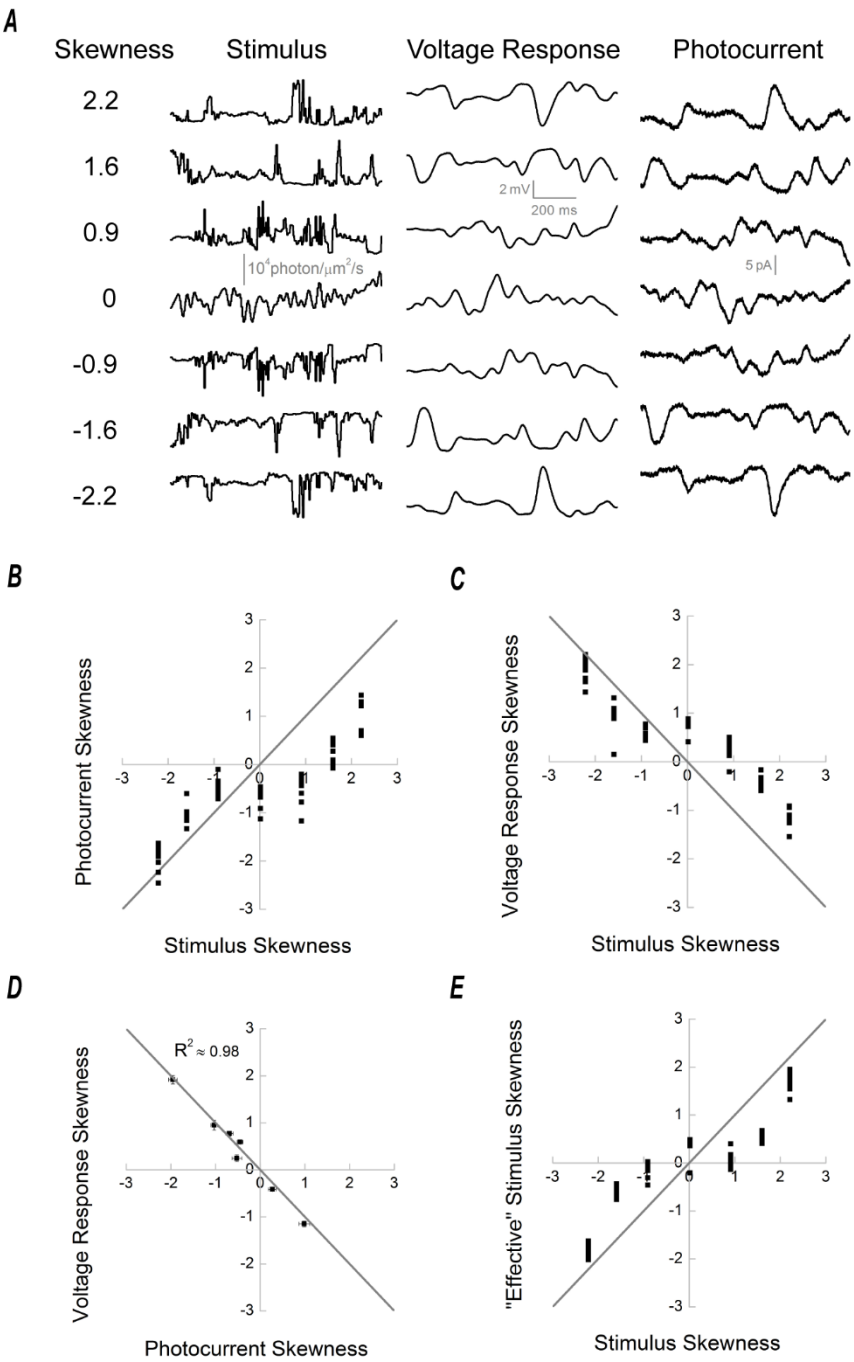

Figure 3

Cone processing affects stimulus skewness. **A.** Skew Stimulus set#1 (left) together with examples of voltage (middle), and photocurrent (right), responses recorded from cone photoreceptors. **B.** Photocurrent skewness as a function of stimulus skewness for Skew Stimulus set #1 (n=8). Each black square represents the skewness of a cell's photocurrent response to a skewed stimulus condition. The grey line depicts the situation where the response skewness is equal to the stimulus skewness. The panel shows cone responses to positive skewed stimuli were less skewed than their stimulus, but to stimuli with zero or negative skews cone responses were more skewed than their stimulus. **C.** Voltage response skewness as a function of stimulus skewness (n=9). Note that the voltage responses and stimuli skews have different sign due to the signal sign-inversion. The grey line describes the situation where response and stimulus skews are equal in magnitude. As was the case in B), cone responses to positive skewed stimuli were less skewed than their stimulus. To stimuli with zero or negative skews, the skewness of the cone's response was

377 greater than that of its stimulus. **D.** Skewness of the voltage response as a function of the photocurrent. For each
378 stimuli condition, the skews of each corresponding voltage response, and photocurrent, were averaged and the
379 resulting means (±SEM) plotted as a voltage response verses photocurrent function. Note that as the cone's voltage
380 response is sign-inverted relative to its photocurrent their skews are also sign inverted. The situation where the
381 voltage response and photocurrent have equal magnitude of skewness is described by the grey line, which fits the
382 data with adjusted R^2 of ≈ 0.98. This indicates that the asymmetric processing of positively and negatively skewed
383 inputs originates in the phototransduction cascade. **E.** "Effective" skewness perceived by the cones as the function
384 of the skewness of the light stimuli. "Effective" skews were estimated from the convolution product of the light
385 stimuli with the cone's impulse response function (Figures 4A&B). The grey line depicts the situation, where
386 "effective" and response skews are equal. Note that for illustrative convenience the "effective" skewness
387 estimated from voltage responses were multiplied by -1. Figure 3E indicates that even though naturalistic stimuli
388 were used, some aspects of the stimuli were still unavailable to drive cone responses on account of the cone's
389 temporal filtering properties. This in turn reduced the range of "effective" skews by almost 30% relative to the
390 original -2.2 to +2.2 range of stimulus skews.

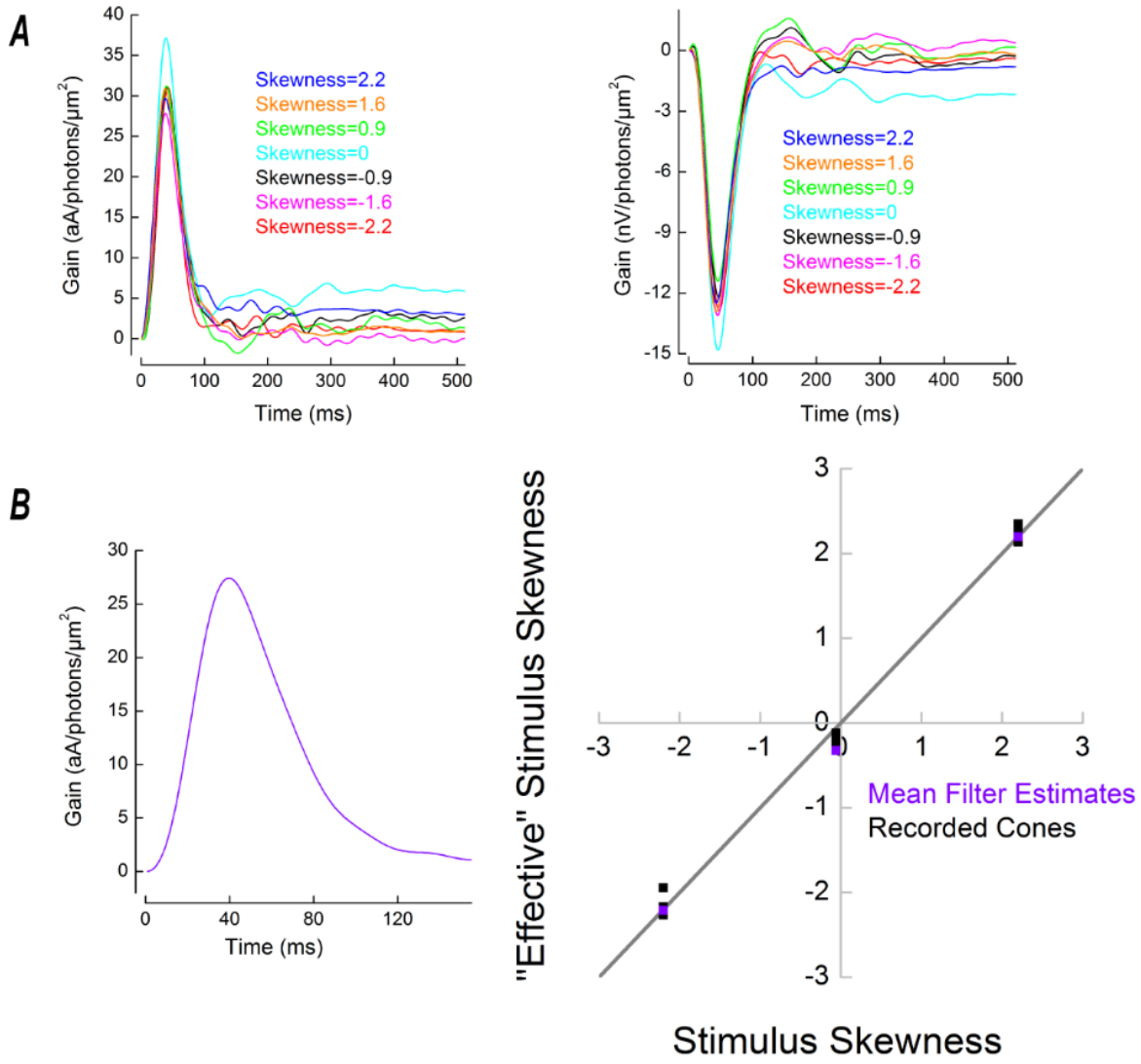

Figure 4

A. Representative examples of the cone impulse response functions obtained using the photocurrent (left) and voltage responses (right) to Skew Stimulus set #1. **B.** Left. The mean cone impulse response function obtained as the averaged photocurrent impulse response functions to all of the stimuli in Skew stimulus set#1 in all of the recorded cells (n=8) (Figure 4A left). This mean photocurrent impulse response function was used, via convolution, to identify segments of the NTSCI where the skewness of the original and "effective" stimuli remained equal, a subsection of which formed Skew stimulus set#2. Right. Skewness of the "effective" stimuli as a function of the skewness of the original stimuli for Skew Stimulus set #2. Violet squares correspond to the "effective" skewness obtained by the convolution of the light stimuli with the mean impulse response function shown on the left. Black squares depict the "effective" skewness 'perceived by each cone under Skew Stimulus set #2 conditions. This was estimated by convolving each Skew Stimulus set #2 stimulus with the cone's impulse

response function obtained for corresponding stimulus. The grey line describes the condition where temporal filtering does not affect stimulus skewness. Since all squares are aligned with the grey line, the "effective" skewness is approximately equal to the original light stimulus skewness. Hence, for Skew Stimulus set #2 cone temporal filtering does not change the skewness delivered by the stimuli.

The processing asymmetry originates exclusively within the phototransduction cascade

What are the cellular mechanisms leading to the differences in the processing of negatively and positively skewed stimuli? To tease apart the relative contributions of the phototransduction cascade and the voltage activated membrane conductances, we plotted the skewness of the voltage responses and photocurrent against each other in Figure 3D. The grey line depicts the condition where photocurrent and voltage response skews are equal in magnitude. All data points fall on this line (R^2 =0.98), meaning that the skewness of the photocurrent accounts for 98% of the skewness of the voltage responses. This means that the phototransduction cascade is the primary source of the asymmetric processing of the positively and negatively skewed stimuli.

Temporal filtering affects stimulus skewness

A cone's finite kinetics may act to temporally filter our light stimulus and thus affect the skewness of the "effective" stimulus perceived by a cone. To determine the "effective" stimuli skews we first estimated the temporal filters of the cone's photocurrent responses to each of the skewed stimuli stretches following the Wiener approach (Wiener, 1964; Rieke, 2001; Figures 4A&B). Next, we convolved the estimated filters with their corresponding skewed stimuli to obtain the "effective" stimuli perceived by cone photoreceptors. Then we calculated the skews of the "effective" stimuli and plotted them against the skews of the original light stimuli in Figure 3E, where the grey line describes the situation where the "effective" skew is

428 equal to the original skew. Data points for the positively skewed light stimuli are lower than
429 the grey line and higher for the negatively skewed light stimuli. Consequently, temporal
430 filtering reduced the "effective" skewness perceived by the cones.

431 Asymmetry in the responses to "effective" stimuli

432 How do goldfish cones process these "effective" stimuli? Figure 3E shows that linear temporal
433 filtering reduces "effective" skewness and decreases the dynamic range over which responses
434 to skewed stimuli were measured by almost 30% (from ±2.2 to ±1.6). Therefore, we first
435 completed our data set by recording the cone's voltage responses to stimuli with "effective"
436 skews of ±2.2 (Figures 4C&5A). Next, we plotted the skews of the responses against the
437 "effective" stimulus skews (Figure 5B) and found that goldfish cones decrease the magnitude
438 of skewness when the stimuli are skewed positively and increase the magnitude of skewness
439 when the stimuli are skewed negatively.
440 Asymmetry in the processing of negatively and positively skewed stimuli is also reflected in
441 the amplitudes of the corresponding responses: standard deviations of the responses to
442 negatively skewed stimuli were up to 50% larger than the standard deviations of the responses
443 to positively skewed stimuli (Figure 5C).

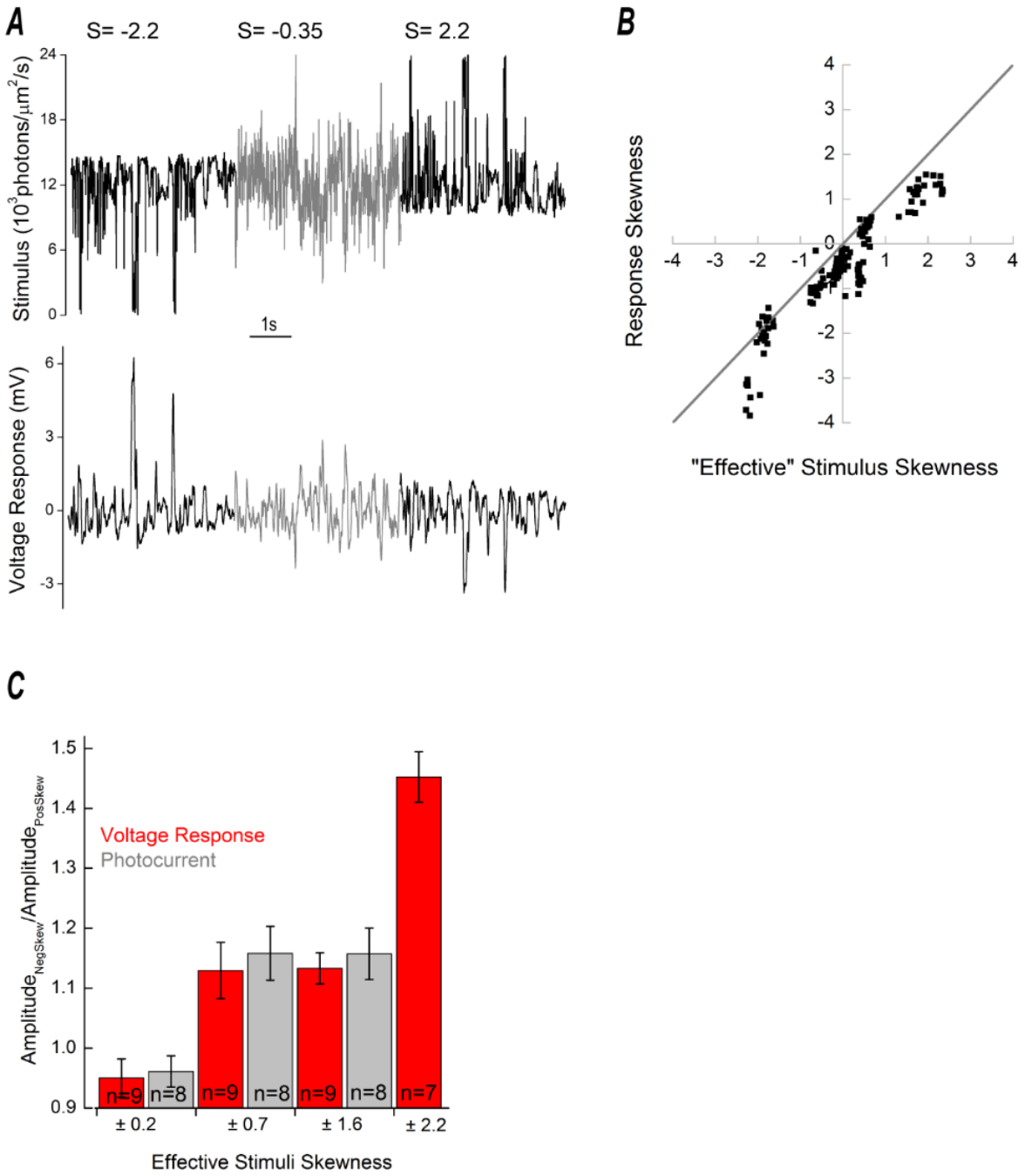

Figure 5

Asymmetries in cone responses to positively and negatively skewed stimuli. **A**. Top. Depiction of Skew Stimulus set #2. The key property of this stimulus set is that the light stimulus skewness is not affected by the temporal filtering properties of cones (Figure 3B). Bottom. An example of a recorded voltage response to Skew Stimulus set #2. **B**. Skews voltage and photocurrent responses against the "effective" stimuli skews. This figure illustrates the relation between "effective" stimulus skew (see Figure 3E, Figure 4B) and the skewness for the photocurrent (n=8) and voltage responses (n=9) of cones stimulated with Skew Stimulus set #1, and the voltage responses of cones (n=7) recorded with Skew Stimulus set #2. This data indicates the cone response skewness differ from the

452 skewness of the “effective” stimulus. Cone responses are less skewed than the stimulus when it delivers higher
453 levels of positive “effective” skew. The opposite occurs when the stimulus delivers higher levels of negative
454 “effective” skew, the cone responses are more skewed than the stimulus. The grey line depicts the situation where
455 the cone response and “effective” stimulus are equally skewed. For illustrative convenience, the voltage responses
456 skews were multiplied by -1. **C**. Differences in cone response amplitudes (photocurrent – grey, voltage response
457 – red) to negatively and positively skewed stimuli for each “effective” skew stimuli pair. When the “effective”
458 skew magnitude was low (±0.2) the photocurrent or voltage responses amplitudes were unaffected by the skew
459 direction. However, at higher “effective” skew-magnitudes cone response amplitudes to negatively skewed stimuli
460 were larger than for positively skewed stimuli (photocurrent difference: ± 0.7, 15.8% ± 4.52% p=0.01; ± 1.6, 15.7
461 ± 4.33% p=0.0083; voltage response difference: ± 0.7, 13.0 ± 4.67% p=0.024; ± 1.6, 13.3 ± 2.64% p=0.0.00097;
462 ± 2.2, 45.2 ± 4.20 % p=0.00004). Changes in response amplitude were assessed as the ratio of standard deviations
463 of a cell’s response to corresponding negatively and positivity skewed stimuli. The “effective” skew values shown
464 were estimated by the mean impulse response (Figure 7), obtained using the impulse response functions of all
465 cells under all stimuli conditions. Data shown as mean ± SEM.

Asymmetry in the cone's output

To be perceived by the downstream neurons, asymmetries in the cone's responses to positively and negatively skewed stimuli (Figures 5B&C) should be reflected in the synaptic release. In photoreceptors, glutamate release is directly proportional to the calcium current (Schmitz & Witkovsky, 1997; Thoreson *et al.*, 2004). Consequently, one can estimate changes in cone glutamate release by recording its calcium current (I_{Ca}).

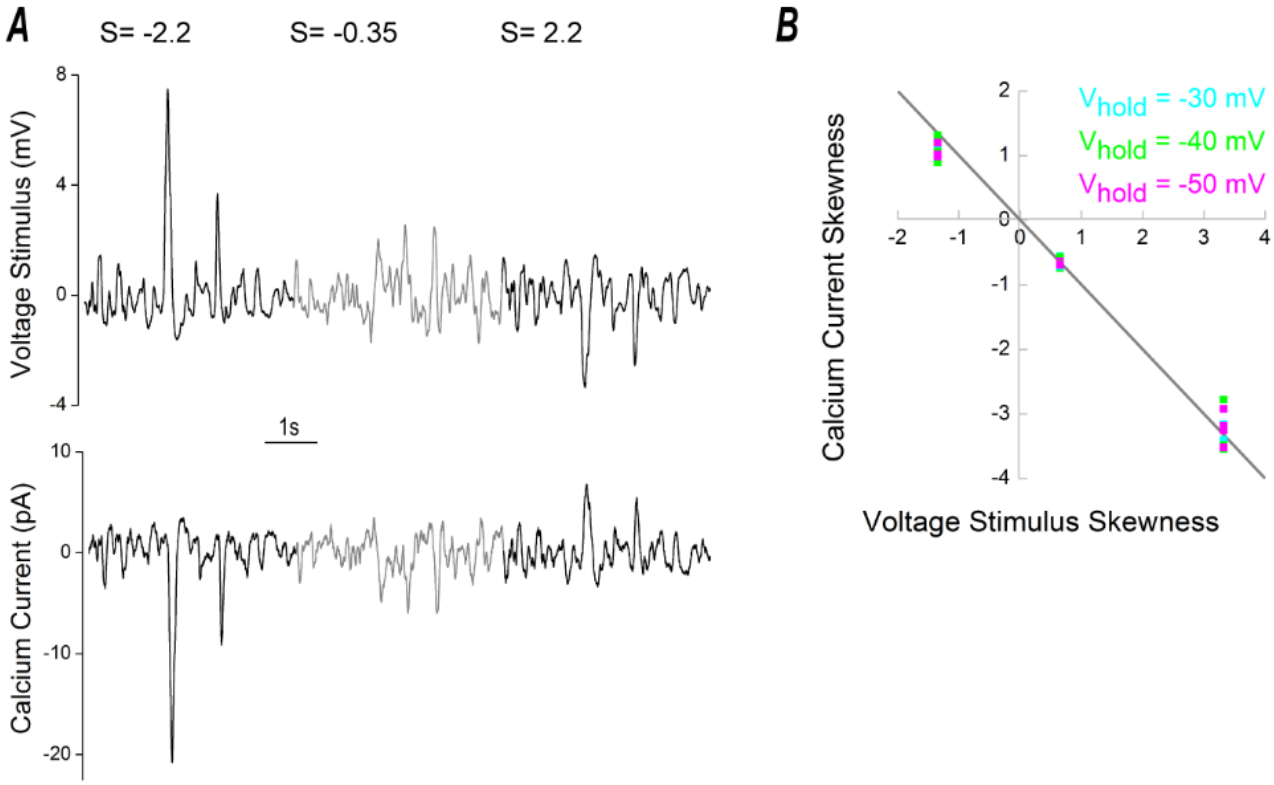

Figure 6

Asymmetrical processing of skewed stimuli at the cone I_{Ca} level. **A.** Top panel depicts the mean cone voltage response to Skew Stimulus set #2, which was used as the stimulus for I_{Ca} measurements. An example I_{Ca} measurement, when using this stimulus, is shown in the bottom panel. **B.** Skewness of I_{Ca} as a function of stimulus skewness. The measurements of I_{Ca} were performed at three different potentials along its activation curve: -30mV (cyan), -40mV (green) and -50mV (magenta). Note that as a decrease in voltage causes an increase in I_{Ca}, skews

480 for the stimulus and response have opposite signs. The grey line denotes the situation where I_{Ca} and its stimulus
481 are equally skewed. Regardless of the holding potential, data points are aligned with grey line, indicating that the
482 cone's I_{Ca} maintains any skewness present in its voltage response. Since cone-photoreceptor glutamate-release is
483 directly proportional to I_{Ca} (Schmitz & Witkovsky, 1997; Thoreson *et al.*, 2004), it is highly likely cone output
484 retains any I_{Ca} skewness.

485

486

487 We measured skew-dependent modulation of I_{Ca} by using recorded voltage responses to light
488 stimuli with "effective" skews of ±2.2 and -0.35 as the command voltages at three different
489 potentials (-30, -40, -50 mV) along the I_{Ca} activation curve (Figure 6A). To isolate I_{Ca}
490 responses, we blocked all other active conductance and subtracted the leak current. We then
491 plotted the skews of the I_{Ca} signals against the skews of the voltage responses (Figure 6B).
492 Note, that since depolarization produces an inward $I_{Ca,}$ the skews of the voltage response and
493 I_{Ca} response have opposite signs.

494 Regardless of the clamping potential, all the data points in Figure 6B approximately fall on the
495 grey line, indicating that the skewness of the cone's signal is largely unaffected by the
496 transformation from membrane potential to the I_{Ca}. Consistent with this, the amplitudes of I_{Ca}
497 during the +2.2 and -2.2 skew conditions differed to the same degree (from 50 ± 1.2% to 54 ±
498 1% depending on the holding potential) as those of the voltage responses (Figure 5C). Thus,
499 for negatively and positively skewed stimuli, the asymmetries present at the cone's earlier
500 processing stages are preserved and even somewhat enhanced in the cone's output.

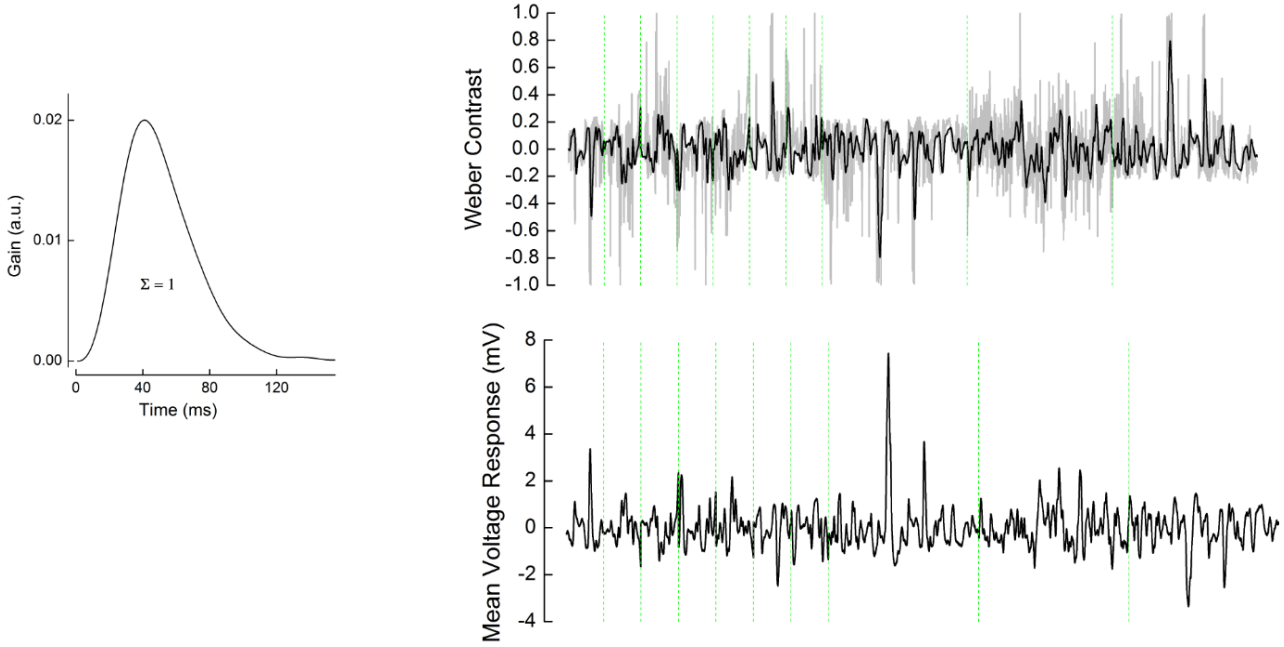

Figure 7

"Effective" Weber contrast steps. Left. Mean impulse response function used to obtain "effective" Weber contrast. The mean impulse response was estimated by averaging the individual voltage-responses impulse-response functions of all cells for all stimuli (n=16) (Figure 4A right, Figure 8B). This mean was scaled such that the integral under its curve was 1. Right. Upper. Grey line: The original light stimuli of Skew Stimulus set #1 and set#2 converted to Weber contrast steps. Black line: The "effective" Weber contrast steps obtained by the convolution of the original Weber contrast steps with the mean impulse response function shown on the left. Bottom. The averaged cone voltage response to each stimuli. For both upper and lower panels, the green dashed lines separate the different stimuli stretches during which the effective skews were (from left to the right): -1.6, -0.2, 0.2, -0.7, 0.06, 1.6, 0.7, -2.2, -0.35, 2.2.

Asymmetrical gain of the cone photoreceptors

What type of non-linear gain leads to the skew-dependent changes in the amplitude of the cone responses? To determine how the voltage response amplitude depends on the Weber contrast step we first converted the "effective" stimuli intensities into Weber contrast steps (Figure 7). Next, we plotted baseline subtracted mean voltage responses (Figure 7) as a function of the

519 “effective” Weber contrast steps (Figure 8A). Figure 8A shows that cone responses are larger
520 for Weber contrast steps below -0.4 than they are for Weber contrast steps above 0.4. Hence,
521 the response gain of cones is greater for high negative, than for high positive, contrasts.

522 What kind of input-output relation supports the asymmetric gain of cones? We fitted the
523 relation between voltage responses and “effective” Weber contrast steps with equation (3)
524 (Figure 8A orange) and found that the cone voltage response is proportional to Weber contrast
525 step with an exponent of -0.1251 ($R^2 \approx 0.95$, 95% confidence interval ± 0.0959). This
526 dependence is close to the one determined in the theoretical study by Van Hateren and Snippe
527 (2006), who suggested that voltage responses of the vertebrate cone is proportional to Weber
528 contrast with an exponent of -0.12.

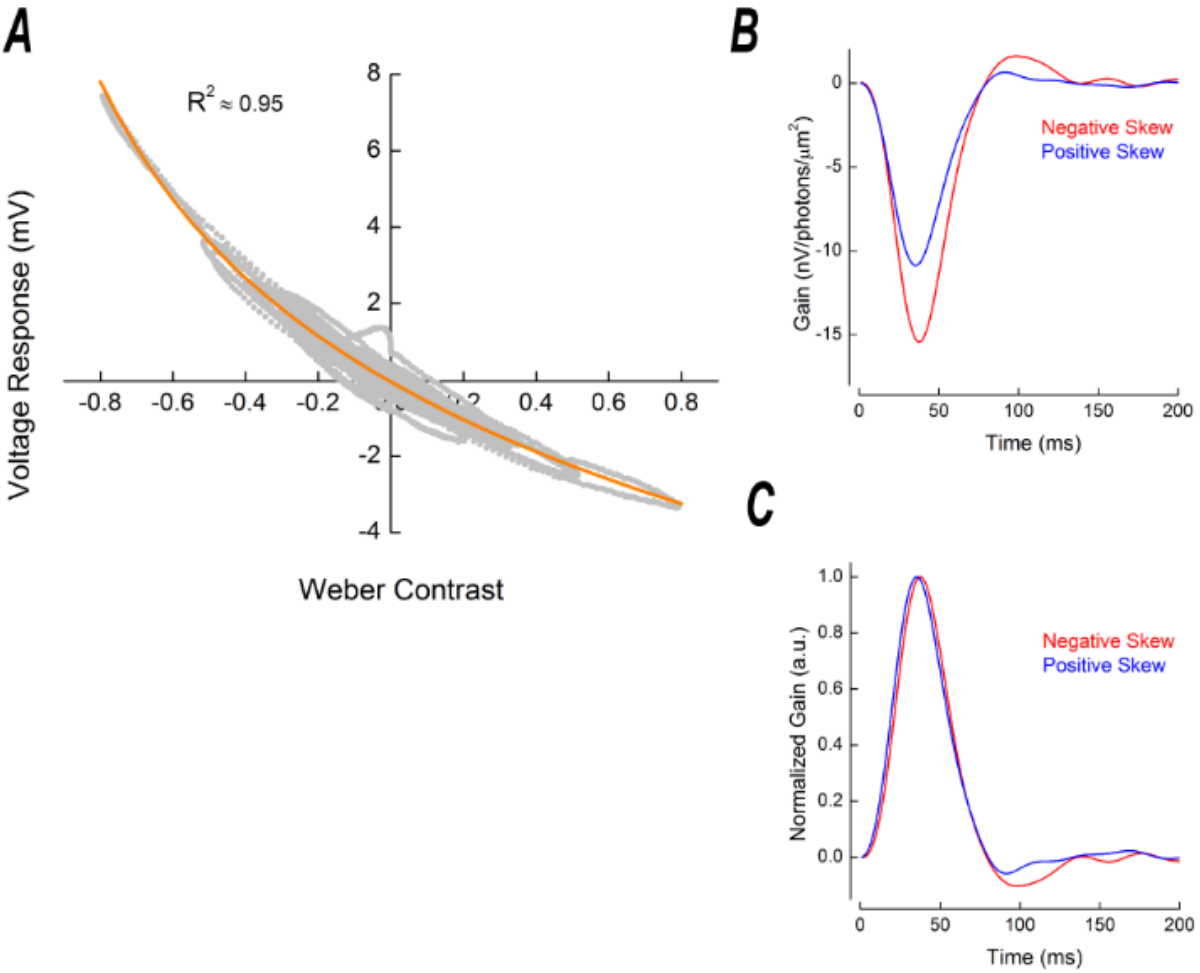

529 **Figure 8**

530 The cone signal transfer properties. **A.** Asymmetric gain of cone photoreceptors. To estimate cone photoreceptor
531 gain, we plotted the voltage response of cones as a function of "effective" Weber contrast. This relationship was
532 well described (orange line, adjusted $R^2 = 0.95$) by the Weber contrast power function given in equation (3) and
533 clearly indicates that cone gain is higher for negative contrasts than for the positive contrasts. The differences
534 become prominent from Weber contrast steps around ±0.4 and are especially vivid for contrast steps beyond ±0.6.
535 "Effective" Weber contrast was obtained by converting the light intensities into Weber contrast steps with
536 equation (2), which were then convoluted with the mean cone impulse response function scaled such that integral
537 under its curve yielded 1 (see methods, Figure 7). The voltage response shown is the baseline-subtracted average
538 of all cells for each stimulus conditions. In total, there are 19000 data points in this figure. **B.** Stimulus skewness
539 changes the shape of the cone's impulse response function. The figure depicts two representative examples of a
540 cone's impulse response function in conditions with -2.2 (red) and +2.2 (blue) "effective'' stimulus skewness. **C.**
541 The cone impulse response functions shown in **B**, normalized by the amplitude of their initial lobe. On average,
542 impulse response functions peaked 3.6 ms, or 9 ± 1.0 %, later for negatively skewed stimulus than for the
543 positively skewed condition ($p=0.0001$, $n=7$) whereas the impulse response function FWHM ($\Delta = 1 \pm 1.35$ %,
544 $p=0.37$, $n=7$) and the cone integration time ($\Delta = 1.1 \pm 1.61$ % ,$p = 0.51$, $n=7$) were unchanged.

545

546 **Stimulus skewness affects the shape of the cone impulse response function**

547 The processing time of cones is inversely proportional to light intensity such that responses to
548 steps of strong positive contrast peak earlier than responses to strong negative contrasts
549 (Nikonov *et al.*, 2000; Lee *et al.*, 2003; van Hateren, 2005; Van Hateren & Snippe, 2006;
550 Angueyra *et al.*, 2021*a*). Therefore, one might expect that such a dependency would lead to a
551 difference in the time courses of the responses to positively and negatively skewed stimuli.

552 To test whether stimulus skewness has an effect on the cone kinetics, we compared impulse
553 response functions derived from the voltage responses to the -2.2 and the +2.2 "effective" skew
554 stimuli (Figure 8B). To better visualize the differences in kinetics we normalized these impulse
555 response functions by the amplitude of their initial lobe (Figure 8C). Interestingly, while on
556 average the cone impulse response functions peaked 3.6 ms (or 9 ± 1.0 %) later for the

557 negatively skewed stimulus than for the positively skewed stimulus (Figure 8C, p=0.0001,
558 n=7), there were no statistically significant differences neither in its full width at the half
559 maximum (FWHM) (Δ = 1.0 ± 1.35 %; p=0.37; n=7), nor in the cone's integration time (Δ=
560 1.1 ± 1.61 %; p=0.51; n=7). This result means that although upon negatively skewed stimuli
561 cone's impulse response function does indeed peak later, this slowdown in the rising flank
562 seems to be compensated by the speedup in the falling flank.

563 Discussion

564 We studied responses of cone photoreceptors to differently skewed stimuli and found cone
565 response amplitudes to negatively skewed stimuli are up to 50% greater than to positively
566 skewed stimuli (Figures 2, 5A&C, 6A, 7). This amplitude difference originates from the
567 asymmetrical weighting of positive and negative contrasts by the phototransduction cascade.
568 Its gain is inversely proportional to Weber contrast steps raised to the power of -0.125 (Van
569 Hateren and Snippe, 2006; Figure 8A) and may serve as the basis for the Blackshot mechanism
570 proposed by Chubb et al. (1994, 2004). Additionally, we observed stimulus skewness changes
571 the cone's impulse response function shape. For the normalized impulse response function, the
572 rising flank was faster and the falling flank slower for positively compared to negatively
573 skewed stimuli (Figure 8C).

574 The Blackshot mechanism

575 Psychophysical studies reported that humans can discriminate visual stimuli based on skewness
576 (Chubb *et al.*, 1994, 2004; Graham *et al.*, 2016). Our results suggest that this discrimination
577 starts as early as the phototransduction cascade. Chubb et al. (1994, 2004) described the
578 sensitivity to skewness with the so-called Blackshot mechanism, which has a disproportionally
579 strong response to high negative contrasts. Our data indicates that differences in the response

580 to positively and negatively skewed stimuli originates in the phototransduction's asymmetric
581 gain function, which leads to higher response amplitudes to negative contrasts than to positive
582 contrasts (Figure 5C, Figure 8A). Moreover, in full accordance with psychophysical studies,
583 the difference in cone response amplitudes to positive and negative contrasts becomes more
584 prominent with larger contrast steps (Figure 8A). For the ±1.6 "effective" skew stimuli pair,
585 where the maximal "effective" Weber contrast step was 0.5, the difference in the response was
586 about 15% while for the ±2.2 "effective" skew pair, where the maximal "effective" Weber
587 contrast step was 0.8, the difference was almost 50% (Figure 5C).

588 Asymmetries in responses to positive and negative contrasts are reported throughout the entire
589 visual system in various species (Laughlin, 1981; Van Hateren, 1997; Lee *et al.*, 2003;
590 Zaghloul *et al.*, 2003; Jin *et al.*, 2008; Yeh *et al.*, 2009; Endeman & Kamermans, 2010; Baden
591 *et al.*, 2013; Kremkow *et al.*, 2014; Cooper & Norcia, 2015), including the human visual cortex
592 (Zemon *et al.*, 1988; Kremkow *et al.*, 2014). Although it was shown that differences in response
593 amplitudes to positive and negative contrasts are additionally amplified by the visual cortex
594 (Kremkow *et al.*, 2014), our data clearly indicates that the primary origin of this asymmetry is
595 within the cone's phototransduction cascade.

596 The phototransduction's asymmetric gain function enables cones to efficiently encode the
597 entire range of contrasts present in natural scenes. Photoreceptors encode changes in their input
598 with a graded output. Information theory states that such a system encodes a signal efficiently
599 only when the statistical distribution of its output is Gaussian, which implies a symmetrical
600 engagement of the system's dynamic range (Shannon, 1948; Van Hateren, 1997). On the other
601 hand, from a given mean, the light intensity cannot decrease by more than 100%, but can easily
602 increase by many orders of magnitude. This means that the dynamic range of positive contrasts
603 is wider than that of negative. Thus, although some visual scenes can be skewed negatively
604 (Tkačik *et al.*, 2014), the total distribution of contrasts at any given intensity is skewed

605 positively with negative contrasts being smaller in amplitude, but more frequent than positive
606 contrasts (Laughlin, 1983; Ruderman, 1994; Van Hateren, 1997; Ruderman *et al.*, 1998;
607 Cooper & Norcia, 2015). Consequently, to encode signals efficiently and to provide
608 symmetrical outputs, cones compensate for this asymmetry in their input by weighting high
609 positive contrasts with lower gain (Figure 8A), such that when stimulated with the entire range
610 of contrasts in natural scenes, cones provide a Gaussian output (Laughlin, 1983; Van Hateren,
611 1997; Endeman & Kamermans, 2010). We therefore suggest that the Blackshot mechanism is
612 simply a consequence of the more fundamental necessity to efficiently encode the range of
613 contrasts present in natural scenes.

614 It is also important to note, that although when it comes to dealing with wide dynamic range
615 of light intensities photoreceptor non-linear gain is well-acknowledged, its influence on
616 perception is often ignored such that responses of the downstream neurons are often modelled
617 with an implicit assumption of the photoreceptor linearity (Chander & Chichilnisky, 2001; Kim
618 & Rieke, 2001; Rieke, 2001; Carandini *et al.*, 2005; Mante *et al.*, 2005; Manookin & Demb,
619 2006; Ozuysal & Baccus, 2012; Pitkow & Meister, 2012; Karamanlis & Gollisch, 2021;
620 Schreyer & Gollisch, 2021). However, there are number of occasions where this non-linearity
621 is important to account for the perceptual features(Kremkow *et al.*, 2014; Angueyra *et al.*,
622 2021*b*). For instance, higher spatial resolution for dark than bright patches is a consequences
623 of the cone photoreceptor non-linear gain (Kremkow *et al.*, 2014). Our data presents another
624 example of the far-reaching consequences of the early visual non-linearity and highlights
625 importance of the account for the photoreceptor non-linearity in studies of the visual system.

626 Shape of the impulse response function

627 We found the cone's impulse response function peaks ≈ 3.6 ms later for negatively skewed
628 stimuli whereas the cone's integration time is unaffected by stimulus skewness (Figure 8B&C).

629 The rising and falling flanks of the cone's impulse response are governed by different
630 biophysical mechanisms. The former is heavily influenced by the phosphodiesterase (PDE)
631 hydrolysis of cGMP. The time constant of this process is inversely proportional to the light
632 intensity. Hence, it decreases upon positive, and increases upon negative contrast steps
633 (Nikonov *et al.*, 2000; van Hateren, 2005; Endeman & Kamermans, 2010). The terminating
634 flank is largely regulated by the guanylyl cyclase (GC) mediated production of cGMP which
635 is modulated by the Ca^{2+} influx through the CNG channels. The time constant of this process
636 is not light-dependent but its gain is inversely proportional to the 4th power of light intensity
637 (Burns et al., 2002; van Hateren, 2005; van Hateren and Snippe, 2007). The interplay between
638 these two underlying processes is thought to account for the cone's impulse response function
639 shape, the asymmetric rising and falling response phases to sinusoidal stimuli, and for light
640 adaptation to decreases in light intensity being slower than for light intensity increases (Baylor
641 & Hodgkin, 1973; Lankheet *et al.*, 1991; Nikonov *et al.*, 2000; Lee *et al.*, 2003; van Hateren,
642 2005; Endeman & Kamermans, 2010; Angueyra *et al.*, 2021*a*).

643 For our stimuli, the PDE hydrolysis of cGMP time-constant will have been shorter during
644 positively skewed stimuli as all large changes in light intensity were associated with positive
645 contrasts. This in turn manifest as a faster rate of change in the impulse response functions'
646 initial flank and hence an earlier time to peak. For negatively skewed stimuli, as all large
647 changes in light intensity were associated with negative contrast, GC mediated production of
648 cGMP was pronounced. The highly non-linear light-dependent gain function of this process,
649 and the ensuing Ca^{2+} influx when cones depolarized, increased the rate the cone CNG channels
650 reopened. This resulted in an increased decay rate for the terminating flank of the impulse
651 response function. Hence, the initial flank's faster onset rate during the positively skewed
652 stimulus is largely offset by the terminating flank's faster decay rate during the negatively

skewed stimulus. Consequently, the cone impulse response function integration time to positive and negative skewed stimuli does not differ while it's time to peak does.

Relation to previous studies using skewed stimuli

Why did previous studies find stimulus skewness had little to no effect on RGC (Tkačik *et al.*, 2014) and LGN neurons (Bonin *et al.*, 2006)? We suggest a methodological factor. In both studies, a large proportion of the stimulus power spectrum was outside the cone's temporal frequency bandwidth. Indeed, Bonin et al. (2006) used white-noise stimuli bandlimited to 124 Hz to study cat LGN neurons responses, while the cat visual system barely responds to frequencies above 32 Hz (Shapley & Victor, 1978; Mante *et al.*, 2005). Similarly, Tkacik et al. (2014) studied salamander RGC responses with white-noise bandlimited to 30 Hz, whereas the salamander retina hardly reacts to frequencies above 10 Hz (Kim & Rieke, 2001). Thus, in both these studies a large part of their stimuli were 'filtered out' and the remaining "effective" stimuli were only able to elicit marginal skew dependent effects.

To illustrate this point, we estimated the "effective" stimuli delivered by Bonin et al. (2006) and Tkacik et al. (2014) using Van Hateren's cone photoreceptor model (van Hateren & Snippe, 2007). Simulations of the cat cone indicate that while a wide range of "effective" Weber contrasts were present (Figure 9A) the "effective" skewness was approximately half that of the original stimuli employed, reducing from a range of ±0.4 to approximately ±0.2 (Figure 9B). Hence, both stimuli delivered largely similar distributions of "effective" Weber contrasts. As a result, the simulated voltage responses to the positive and negatively skewed stimuli only differed in amplitude by approximately 4% (Figure 9 C, D), which is within the range of standard error estimates for the amplitude differences we find here (Figure 5C).

Simulations of the salamander cone reveal a different situation that none the less leads to the same outcome. The "effective" skewness range remained relatively large despite being less

than half that of the original stimuli employed (±0.8 vs ±2, Figure 10B), but the range of "effective" contrasts reduced to just ±0.2 Weber unit (Figure 10A). Over this limited range of contrasts the cone photoreceptor gain is mostly symmetrical (Figure 8A) and as such the voltage response amplitude to the negatively skewed stimulus was only 2% higher than for the positively skewed stimulus (Figure 10C&D). Hence, even though the stimuli had substantially different distributions of "effective" Weber contrasts, the range of contrast values they delivered were too narrow to generate a notable effect.

To conclude, our results show that to study visual processes under varying skewness conditions, the stimuli must be able to deliver sufficient levels of "effective" skewness over sufficient ranges of "effective" Weber contrasts.

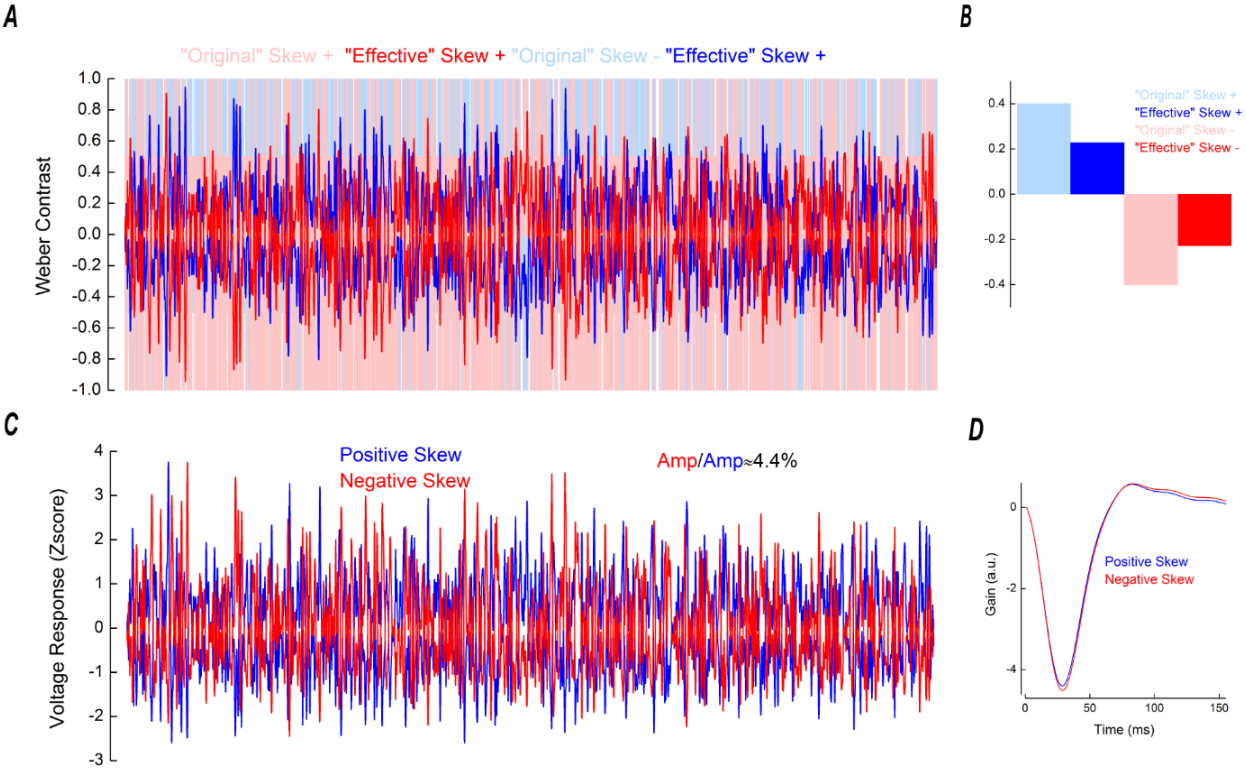

Figure 9

Simulated responses of cat cone photoreceptors. **A.** Light blue and light red lines depict the positively and negatively skewed stimuli used by Bonin et al. (2006) and here for the simulation. Blue and red lines depict the "effective" positively and negatively skewed stimuli, obtained by the convolution of the "original" stimuli with

the impulse response functions shown in **D**. **B.** Comparison of the skews of the "original" and "effective" positively (blue) and "negatively" (red) skewed stimuli. Due to the temporal filtering the "effective" stimuli are almost symmetrical around the mean, their skew range having decreased from ±0.4 to ≈ ±0.2. **C.** Simulated cone voltage responses to the positively (blue) and negatively (red) skewed stimuli. The response amplitude to the negatively skewed stimulus was 4% higher than the response amplitude to the positively skewed stimulus. The simulated voltage response amplitudes were quantified by their standard deviations, as for Figure 5C. Parameters for the simulation are listed in the Table 1. **D.** Impulse response functions derived from the simulated cat cone voltage responses. These impulse response functions were used to estimate the "effective" stimuli shown in **A.**

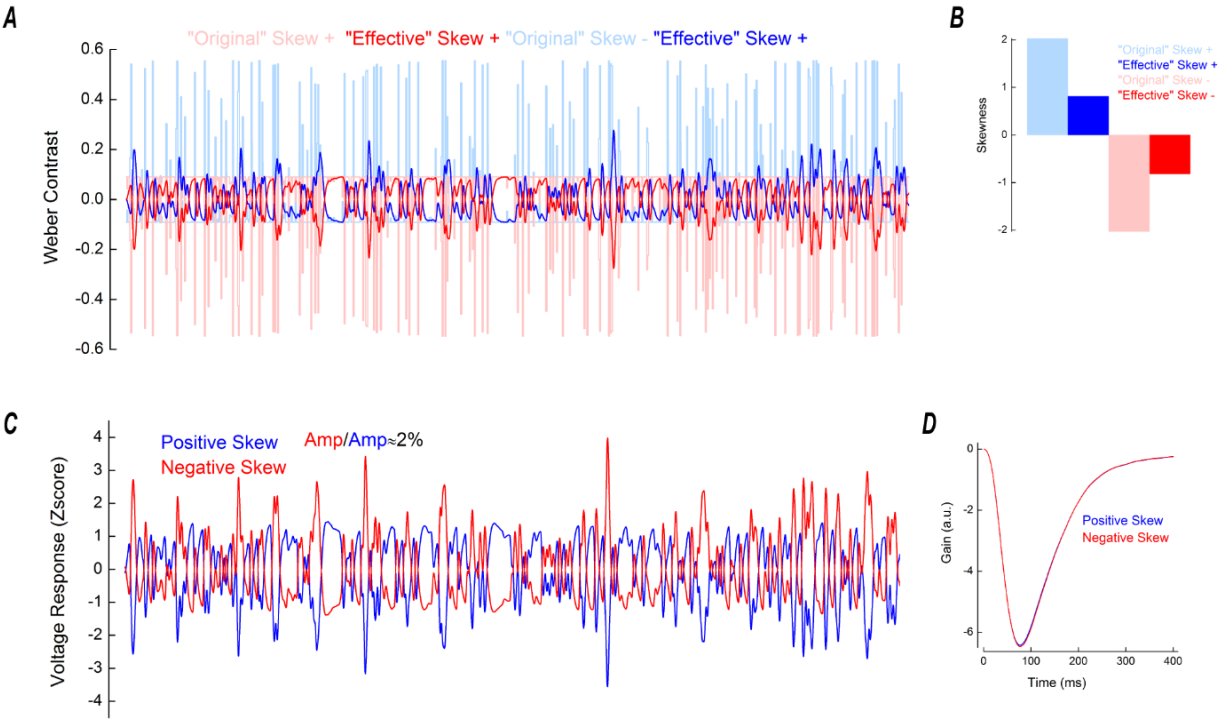

Figure 10

Simulated responses of salamander cone photoreceptors. **A.** Light blue and light red lines depict the positively and negatively skewed stimuli used in the simulation. These stimuli had the same properties as those used by Tkacik et al.(2014). Blue and red lines depict the "effective" positively and negatively skewed stimuli, obtained by the convolution of the "original" stimuli with the impulse response functions shown in **D**. The temporal filtering leads to small Weber contrast ranges of the "effective" stimuli. **B.** Comparison of the skews of the "original" and "effective" positively (blue) and "negatively" (red) skewed stimuli. The salamander cone's temporal filtering reduced the stimulus skewness from ±2 to ±0.8. **C.** Simulated cone voltage responses to the positively (blue) and negatively (red) skewed stimuli. The response amplitude to the negatively skewed stimulus was 2% higher than the response amplitude to the positively skewed stimulus. The simulated voltage response amplitudes were

quantified by their standard deviations, as for Figure 5C. Parameters for the simulation are listed in the Table 1. **D.** Impulse response functions derived from the simulated salamander cone voltage responses. These impulse response functions were used to estimate the "effective" stimuli shown in **A.**

References

Angueyra JM, Baudin J, Schwartz GW & Rieke F (2021*a*). Multiple time scales of adaptation allow cones to encode the inputs created by visual exploration of natural scenes. *bioRxiv*2021.02.13.431101.

Angueyra JM, Baudin J, Schwartz GW & Rieke F (2021*b*). Multiple time scales of adaptation allow cones to encode the inputs created by visual exploration of natural scenes. 1–39.

Baccus SA & Meister M (2002). Fast and slow contrast adaptation in retinal circuitry. *Neuron* **36,** 909–919.

Baden T, Schubert T, Chang L, Wei T, Zaichuk M, Wissinger B & Euler T (2013). A tale of two retinal domains: Near-Optimal sampling of achromatic contrasts in natural scenes through asymmetric photoreceptor distribution. *Neuron* **80,** 1206–1217.

Baylor DA & Hodgkin AL (1973). Detection and resolution of visual stimuli by turtle photoreceptors. *J Physiol* **234,** 163–198.

Bonin V, Mante V & Carandini M (2006). The statistical computation underlying contrast gain control. *J Neurosci* **26,** 6346–6353.

Burns ME, Mendez A, Chen J & Baylor DA (2002). Dynamics of cyclic GMP synthesis in retinal rods. *Neuron* **36,** 81–91.

Carandini M, Demb JB, Mante V, Tolhurst DJ, Dan Y, Olshausen BA, Gallant JL & Rust NC (2005). Do we know what the early visual system does? *J Neurosci* **25,** 10577–10597.

Chander D & Chichilnisky EJ (2001). Adaptation to Temporal Contrast in Primate and Salamander Retina. *J Neurosci* **21,** 9904–9916.

Chichilnisky EJ (2001). A simple white noise analysis of neuronal light responses. *Netw Comput Neural Syst* **12,** 199–213.

Chubb C, Econopouly J & Landy MS (1994). Histogram contrast analysis and the visual segregation of IID textures. *J Opt Soc Am A* **11,** 2350.

Chubb C, Landy MS & Econopouly J (2004). A visual mechanism tuned to black. *Vision Res* **44,** 3223–3232.

Cooper EA & Norcia AM (2015). Predicting Cortical Dark/Bright Asymmetries from Natural Image Statistics and Early Visual Transforms. *PLoS Comput Biol* **11,** 1–25.

Daly SJA & Normann R (1985). Temporal Information Processing In Cones: Effects of Light Adaptation on Temporal Summation and Modulation. *Vision Res* **25,** 1197–1206.

Donner K & Hemila S (1996). Modelling the spatio-temporal modulation response of ganglion cells with difference-of-Gaussians receptive fields: Relation to photoreceptor response kinetics. *Vis Neurosci* **13,** 173–186.

Endeman D & Kamermans M (2010). Cones perform a non-linear transformation on natural stimuli. *J Physiol* **588,** 435–446.

Fahrenfort I, Habets RL, Spekreijse H & Kamermans M (1999). Intrinsic cone adaptation modulates feedback efficiency from horizontal cells to cones. *J Gen Physiol* **114,** 511–524.

Frazor RA & Geisler WS (2006). Local luminance and contrast in natural images. *Vision Res* **46,** 1585–1598.

Graham D, Schwarz B, Chatterjee A & Leder H (2016). Preference for luminance histogram regularities in natural scenes. *Vision Res* **120,** 11–21.

van Hateren H (2005). A cellular and molecular model of response kinetics and adaptation in primate cones and horizontal cells. *J Vis* **5,** 331–347.

Van Hateren JH (1997). Processing of natural time series of intensities by the visual system of the blowfly. *Vision Res* **37,** 3407–3416.

Van Hateren JH, Rüttiger L, Sun H & Lee BB (2002). Processing of natural temporal stimuli by macaque retinal ganglion cells. *J Neurosci* **22,** 9945–9960.

van Hateren JH & Snippe HP (2007). Simulating human cones from mid-mesopic up to high-photopic luminances. *J Vis* **7,** 1.

Van Hateren JH & Snippe HP (2006). Phototransduction in primate cones and blowfly photoreceptors: Different mechanisms, different algorithms, similar response. *J Comp Physiol A Neuroethol Sensory, Neural, Behav Physiol* **192,** 187–197.

Howlett MHC, Smith RG & Kamermans M (2017). A novel mechanism of cone photoreceptor adaptation. *PLoS Biol* **15,** e2001210.

Jin JZ, Weng C, Yeh CI, Gordon JA, Ruthazer ES, Stryker MP, Swadlow HA & Alonso JM (2008). On and off domains of geniculate afferents in cat primary visual cortex. *Nat Neurosci* **11,** 88–94.

Kamar S, Howlett MHC & Kamermans M (2019). Silent-substitution stimuli silence the light responses of cones but not their output. *J Vis* **19,** 1–11.

Kamermans W, Ariette M, Farajnia S, Howlett M & Kamermans M (2017). A quantitative model for adaptation of in cone photoreceptors to contrast. ; DOI: 10.6084/m9.figshare.12813191.v1. Available at:

https://figshare.com/articles/poster/A_quantitative_model_for_adaptation_of_in_cone_photoreceptors_to_contrast/12813191.

Karamanlis D & Gollisch T (2021). Nonlinear spatial integration underlies the diversity of retinal ganglion cell responses to natural stimuli. **41,** 3479–3498.

Kim KJ & Rieke F (2001). Temporal contrast adaptation in the input and output signals of salamander retinal ganglion cells. *J Neurosci* **21,** 287–299.

Korenberg MJ (1991). Parallel cascade identification and kernel estimation for nonlinear systems. *Ann Biomed Eng* **19,** 429–455.

Kremkow J, Jin J, Komban SJ, Wang Y, Lashgari R, Li X, Jansen M, Zaidi Q & Alonso JM (2014). Neuronal nonlinearity explains greater visual spatial resolution for darks than lights. *Proc Natl Acad Sci U S A* **111,** 3170–3175.

Lankheet MJM, van Wezel RJA & van de Grind WA (1991). Light adaptation and frequency transfer properties of cat horizontal cells. *Vision Res* **31,** 1129–1142.

Laughlin S (1981). A simple coding procedure enhances a neuron's information capacity. *Zeitschrift fur Naturforsch - Sect C J Biosci* **36,** 910–912.

Laughlin S (1983). Matching Coding to Scenes to Enhance Efficiency. 42–52.

Lee BB, Dacey DM, Smith VC & Pokorny J (2003). Dynamics of sensitivity regulation in primate outer retina: The horizontal cell network. *J Vis* **3,** 513–526.

Malchow RP & Yazulla S (1986). Separation and light adaptation of rod and cone signals in the retina of the goldfish. *Vision Res* **26,** 1655–1657.

Manookin MB & Demb JB (2006). Presynaptic Mechanism for Slow Contrast Adaptation in Mammalian Retinal Ganglion Cells. *Neuron* **50,** 453–464.

Mante V, Frazor RA, Bonin V, Geisler WS & Carandini M (2005). Independence of luminance and contrast in natural scenes and in the early visual system. *Nat Neurosci* **8,** 1690–1697.

Nikonov S, Lamb TD & Pugh EN (2000). The role of steady phosphodiesterase activity in the kinetics and sensitivity of the light-adapted salamander rod photoresponse. *J Gen Physiol* **116,** 795–824.

Ozuysal Y & Baccus SA (2012). Linking the Computational Structure of Variance Adaptation to Biophysical Mechanisms. *Neuron* **73,** 1002–1015.

Pitkow X & Meister M (2012). Decorrelation and efficient coding by retinal ganglion cells. *Nat Publ Gr* **15,** 628–635.

Rieke F (2001). Temporal contrast adaptation in salamander bipolar cells. *J Neurosci* **21,** 9445–9454.

Ruderman DL (1994). The statistics of natural images. *Netw Comput Neural Syst* **5,** 517–548.

Ruderman DL, Cronin TW & Chiao C-C (1998). Statistics of cone responses to natural images: implications for visual coding. *J Opt Soc Am A* **15,** 2036.

Schmitz Y & Witkovsky P (1997). Dependence of photoreceptor glutamate release on a dihydropyridine- sensitive calcium channel. *Neuroscience* **78,** 1209–1216.

Schreyer HM & Gollisch T (2021). Nonlinear spatial integration in retinal bipolar cells shapes the encoding of artificial and natural stimuli. *Neuron* **109,** 1692-1706.e8.

Shannon CE (1948). A Mathematical Theory of Communication. **27,** 379–423.

Shapley RM & Victor JD (1978). The effect of contrast on the transfer properties of cat retinal ganglion cells. *J Physiol*275–298.

Simoncelli EP, Pillow JW, Paninski L & Schwartz O (2004). Characterization of Neural

Responses with Stochastic Stimuli.

Student (1908). The probable Error of a Mean. *Biometrika* **6,** 1–25.

Thoreson WB, Rabl K, Townes-Anderson E & Heidelberger R (2004). A highly Ca2+-sensitive pool of vesicles contributes to linearity at the rod photoreceptor ribbon synapse. *Neuron* **42,** 595–605.

Tkačik G, Ghosh A, Schneidman E & Segev R (2014). Adaptation to changes in higher-order stimulus statistics in the salamander retina. *PLoS One*; DOI: 10.1371/journal.pone.0085841.

Vroman R, Klaassen LJ, Howlett MHC, Cenedese V, Klooster J, Sjoerdsma T & Kamermans M (2014). Extracellular ATP Hydrolysis Inhibits Synaptic Transmission by Increasing pH Buffering in the Synaptic Cleft. *PLOS Biol* **12,** e1001864.

Welch PD (1967). Welchs Periodogram.pdf. *IEEE Trans Audio Electroacoust* **15,** 70–73.

Wiener N (1964). *Extrapolation, Interpolation, and Smoothing of Stationary Time Series*. The MIT Press.

Yeh CI, Xing D & Shapley RM (2009). “Black” responses dominate macaque primary visual cortex V1. *J Neurosci* **29,** 11753–11760.

Zaghloul KA, Boahen K & Demb JB (2003). Different circuits for ON and OFF retinal ganglion cells cause different contrast sensitivities. *J Neurosci* **23,** 2645–2654.

Zemon V, Gordon J & Welch J (1988). Asymmetries in ON and OFF visual pathways of humans revealed using contrast-evoked cortical potentials. *Vis Neurosci* **1,** 145–150.

843 **Table 1**

Parameter	Goldfish	Cat	Salamander
Lifetime of activated conopsin	8 – 31 ms	8 ms	88 ms
Lifetime of activated transducin	16 – 30 ms	12 ms	101 ms
Dark PDE activity	0.003 ms^{-1}	0.0028 ms^{-1}	0.003 ms^{-1}
Constant of the dependence of PDE activity on transducin activation	0.00004 - 0.00023	0.00016	0.0002
Apparent Hill coefficient of CNG channels	1	1	1
Hill coefficient of GC activation	4	4	4
Time constant of calcium extrusion	12 -28 ms	9 ms	24 ms
GC activation constant	0.1	0.09	0.1
Capacitive membrane time constant	15 ms	6 ms	15 ms
Parameter of membrane non-linearity	0.7 – 1.1	0.8	0.85
Constant of membrane nonlinearity	0.03 – 0.07	0.07	0.085
Time constant of membrane non-linearity	300 ms	120 ms	300 ms

844

845 Parameters of the Van Hateren model used to simulate the responses of goldfish, salamander

846 and cat cones. For the goldfish, model parameters were obtained by fitting cones responses

847 (n=7) to Skew Stimulus Set #2 while constraining the range the parameters varied to within

848 that determined by Endeman and Kamermans (2010). For the cat and salamander, parameters

849 were adjusted such that the simulated-cone's impulse response function time-to-peak

850 approximately matched that estimated, respectively, by Donner and Hemila (1996) and by

851 Rieke (2001) and Baccus and Meister (2002).